Journal of the European Ceramic Society 20 (2000) 1231–1240

Influence of vanadium substitution on sintering behaviour of $Pb_3(VO_4)_{2(1-x)}(PO_4)_{2x}$ ceramics

Thierry Robin[a], Didier Bernache-Assollant[a,*], Fabienne Audubert[b]

[a]*SPCTS, UMR 6638, 123 Avenue A. Thomas, 87060 Limoges Cedex, France*
[b]*CEA DCC/DESD/SEP/LEMC, Centre d'Études Nucléaires de Cadarache, 13108 St-Paul lez Durance, France*

Received 23 July 1999; received in revised form 26 October 1999; accepted 31 October 1999

Abstract

Intermediate-stage sintering has been investigated in lead orthophosphovanadates $Pb_3(VO_4)_{2(1-x)}(PO_4)_{2x}$. It was found that rich-vanadium compounds such as $Pb_3(VO_4)_2$ and $Pb_3(VO_4)_{1.6}(PO_4)_{0.4}$ densify rapidly with important grain growth. For these compounds grain growth is controlled by grain boundaries and densification occurs by a mixed mechanism with lattice and grain boundary diffusion. For $Pb_3(PO_4)_2$, sintering mechanism supports a model of grain-boundary-controlled densification and grain growth is a surface diffusion-controlled pore drag mechanism. Moreover, the presence of phosphorus in compounds' formulae, tends to decrease the grain-boundary mobility, preventing pore-boundary separation. The kinetics analysis highlights the importance of vanadium substitution in modifying the diffusion coefficient of rate-limiting species.

Keywords: Grain boundaries; Grain growth; $Pb_3(PO_4,VO_4)_2$; Sintering

1. Introduction

Most sintering studies are made on typical materials such as oxides, carbides or nitrides. A small quantity of ceramics are also studied for their specific properties which require a particular knowledge. In fact, many desired properties of ceramics are related to their microstructures. It belongs to sintering studies to link properties and microstructures in revealing the predominant densification and grain growth mechanisms that occur during heat treatment.

Apatites form a large family of mineral compounds of the general formula $Me_{10}(XO_4)_6Y_2$, whose fluorapatite $Ca_{10}(PO_4)_6F_2$ is the most abundant natural phase. Important studies on several natural apatites have lead towards the choice of this class of minerals as a new potential material for the confinement of separated elements,[1] especially because of numerous substitutions, both in anionic and cationic sites. Indeed, among the different elements, introduction of big ions such as iodine in the apatitic cell is possible with respect to the steric bulk and chemistry conditions, in using voluminous cations and tetrahedral groups. So, $Pb_3(VO_4)_{2(1-x)}(PO_4)_{2x}$ ceramics can be used as a conditioning matrix for iodine, producing apatite: $3Pb_3(VO_4)_{2(1-x)}(PO_4)_{2x} + PbI_2 \rightarrow Pb_{10}(VO_4)_{6(1-x)}(PO_4)_{6x}I_2$, as shown in previous works.[2–4] While the presence of vanadium increases the crystal cell volume, permitting iodine introduction in apatitic cell, phosphor reduces the phase transition of $Pb_3(VO_4)_2$ below the ambient temperature. The aim of this work consists in optimising the sintering process, especially in reducing the sintering temperature. In order to sinter at the lowest temperature as possible, the main objective is necessarily the comprehension of sintering behaviour. Each part of the ceramic process needs a special study, like the grinding conditions for powder preparation.[5] In this work, the operative procedure begins with the powders synthesis and ends with the sintering mechanisms determination. Particular attention is focused on vanadium substitution to define more correctly in the future the final composition with the best adapted microstructure.

2. Experimental procedure

2.1. Powder preparation

$Pb_3(VO_4)_{2(1-x)}(PO_4)_{2x}$ powder samples were prepared by calcining PbO, V_2O_5 and $NH_4H_2PO_4$ (Prolabo) in

* Corresponding author. Fax: +33-5545-7586.
E-mail address: bernache@unilim.fr (D. Bernache-Assollant).

0955-2219/00/$ - see front matter
PII: S0955-2219(99)00289-7

the appropriate proportions for three different degrees of substitution: $x=0$, $x=0.2$ and $x=1$. $Pb_3(VO_4)_2$, i.e. when $x=0$, is the compound used as a reference when comparing the different compositions. Before heating, powder reactants were dry mixed in a turbula during 24 h. The mixture was molten in a platinum crucible at 1000°C in air during 1 h.[6] Melts were then cooled down to room temperature with a speed of 300°C/h.

The yellow-coloured solid samples were ground in a mortar and then the powders were milled in an attritor, together with distilled water, by rubbing Zirconia grinding balls of 1 and 2 mm in diameter with a rotating Nylon impeller at a speed of 450 rd.min^{-1}, during 3 up to 5 h. After drying, powders were sieved to 63 μm.

2.2. Powder compacts

The attrition-milled powders were dry-pressed ranging from 100 to 125 MPa into pellets in a stainless steel die to 10 mm in diameter and 2 mm thick. The geometrical measured green densities after pressing were $60\pm1\%$ of the theoretical density, according to the composition.

2.3. Densification studies

Sintering was performed in air using a vertical furnace for isothermal treatments. A fast-firing method was used to reach the desire temperature of 650°C, with a system for pulling down samples through the furnace at a speed of 20 cm/min. Samples were held from 0 up to 900 min, and pulled out through at the same speed to room temperature. The aim of this sintering method is to avoid low temperature non-densifying mechanisms able to strongly modify the microstructure of $Pb_3(VO_4)_{2(1-x)}(PO_4)_{2x}$ samples.[5]

2.4. Characterisation

Measurements of theoretical densities of each compound were performed by X-ray diffraction (Siemens D5000 and U_fit software) and He-pycnometry using a AccuPyc 1330 from Micromeritics. Theoretical density, $\rho_{th}=7.302$, of the solid solution $Pb_3(VO_4)_{1.6}(PO_4)_{0.4}$ ($x=0.2$) was calculated using Vegard's law with $\rho_{th}=7.248$ for $Pb_3(VO_4)_2$ and $\rho_{th}=7.52$ for $Pb_3(PO_4)_2$.

Surface area (S_{BET}) was measured using an ASAP 2010 from Micromeritics. This apparatus is based on nitrogen adsorption at 77 K, using BET equation. Powder size distribution was measured with a laser granulometer CILAS 1064, using distilled water as the medium.

Sintered bulk densities were determined by the Archimedes method with distilled water as the immersion medium. The microstructures were characterised by a scanning electron microscope (Hitachi S2500). Neither chemical nor thermal treatments were used to reveal the microstructure. The average grain size, G, was measured for all sintered samples using the linear intercept technique, with OptiLab^{TM}/Pro-F2.6.1 Graftek image analysis software. The value of G is obtained by multiplying the average intercept length, L, of at least 300 grains, by 1.56.[7] This value is identical wherever the measure is made, either on the sample surface or on the polished zone.

3. Results

3.1. Powder characterisation

After synthesis, no secondary phases are found on X-ray profiles of well-crystallised powders. There is no significant variations from JCPDS patterns and Vegard's law result between calculated and measured theoretical densities for the three compounds. At room temperature, $Pb_3(VO_4)_{1.6}(PO_4)_{0.4}$ crystallises in a rhombohedral γ phase with the space group $R\bar{3}m$ whereas $Pb_3(VO_4)_2$ and $Pb_3(PO_4)_2$ crystallise in a monoclinic β phase with space group $P2_1/c$ for $Pb_3(VO_4)_2$[8] and C2 for $Pb_3(PO_4)_2$.[9] A phase transition from high-temperature rhombohedral phase to low-temperature monoclinic phase undergoes at $T_{\beta\rightarrow\gamma}=100$°C for $Pb_3(VO_4)_2$ and $T_{\beta\rightarrow\gamma}=180$°C for $Pb_3(PO_4)_2$.

SEM observation illustrates that particles morphology can not be characterised by a specific geometrical form, whatever the composition is (Fig. 1).

The size distributions are broad and some significant agglomerates can be seen from the micrographs, especially for $Pb_3(PO_4)_2$ [Fig. 1(c)]. Nevertheless, the three size distributions are characterised by similar average particle diameter, $Ø_{50}$, and BET equivalent spherical diameter d_{BET}, illustrating a good agreement between the 3 different compositions. Powder characteristics are listed in Table 1.

3.2. Densification behaviour

Fig. 2 shows the relative density, ρ, versus time for the 3 compounds. Each point was taken from a separate sample. The curves through the experimental data were plotted in the form of a polynomial law where time was measured in minutes once samples reached $T=650$°C.

On one hand, the plots for $Pb_3(VO_4)_{1.6}(PO_4)_{0.4}$ and $Pb_3(VO_4)_2$ show that densification begin during heating of the sample, before desired temperature of 650°C is attained, and reached 95% of theoretical density in 20 min [Fig. 2(a)]. On the other hand, $Pb_3(PO_4)_2$ needed more than 900 min at the same temperature to reach a relative density less than 90% of the theoretical one, as shown in Fig. 2(b). Relative low end-point density observed for $Pb_3(PO_4)_2$ samples — several percentages lower in fact than those obtained for the 2 other compositions at the same time — are clearly shown in Fig.

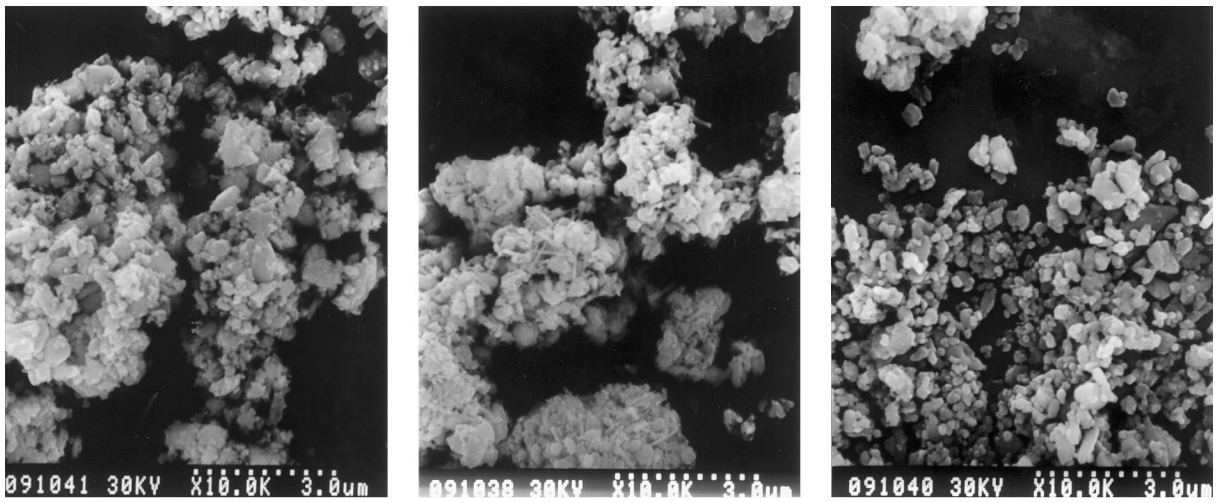

(a) (b) (c)

Fig. 1. SEM micrographs of (a) $Pb_3(VO_4)_{1.6}(PO_4)_{0.4}$, (b) $Pb_3(VO_4)_2$ and (c) $Pb_3(PO_4)_2$ powders, respectively.

Table 1
Density, specific surface area and size characteristics of powder used in this study

Sample	Theoretical density	S_{BET} ($m^2.g^{-1}$)	d_{BET} (μm)	$\varnothing_{50}$ (μm)
$Pb_3(VO_4)_{1.6}(PO_4)_{0.4}$	7.302	6.2 ± 0.1	0.132 ± 0.05	0.8
$Pb_3(VO_4)_2$	7.248	6.0 ± 0.1	0.138 ± 0.02	1.0
$Pb_3(PO_4)_2$	7.520	4.3 ± 0.1	0.186 ± 0.04	1.0

2(a). Moreover, fast densification which begins during the early stage of sintering acts together with rapid coalescence of small particles into larger ones, as we pointed out in a former work.[5] Indeed, above 400°C, surface area reduction with grain coalescence begin to be significant, reducing powder reactivity.

3.3. Grain growth behaviour

Micrographs of some microstructure development for samples made from each powder at different sintering times are shown in Fig. 3. Magnifications used for $Pb_3(PO_4)_2$ are taken as reference to compare grain growth between the three different compounds. As shown in Table 1, whatever the compound is, the average grain sizes before sintering are quite identical. The difference in grain growth behaviour can be easily seen then. No abnormal grain growth has taken place in all the cases studied. Despite a large difference in mean grain after sintering, the majority of grains had a size centred around the mean. Moreover, Fig. 4 shows the conservation of grain size distribution; grain growth of $Pb_3(VO_4)_{2(1-x)}(PO_4)_{2x}$ is, therefore, normal during sintering at 650°C. Whatever the sintering time, all grain distributions follow the same curve. This allowed the use of the linear intercept length, L, to represent the grain size for all the samples. Fig. 5 shows the dependence of the average grain size on the sintering time at 650°C. The curves through the data were obtained from a polynomial fit of grain size versus time.

4. Discussion

4.1. Densification kinetics

The influence of density on the rates of densification for $Pb_3(VO_4)_{2(1-x)}(PO_4)_{2x}$ powder compacts are reported in Fig. 6. The plots are linear up to a boundary region between 88 and 90% of the theoretical density. A sharp downturn in plots of $Pb_3(VO_4)_2$ and $Pb_3(VO_4)_{1.6}(VO_4)_{0.4}$ samples are observed, whilst the plot of $Pb_3(PO_4)_2$ densification rate is linear. It is suitable to define the boundary region, following Gupta,[10] as a density zone between intermediate- and final-stage sintering. In this density range, the pore network breaks into short segments leading to the formation of isolated pores.

Shiau et al.[11] showed that low variations in particle-size distribution have an effect on the evolution of pore channel. Indeed, for a narrow distribution without agglomerates, pore network in high-purity alumina powder compacts start to break up at 91% relative density, whereas with a larger grain-size distribution, porosity pinches off earlier, at 86% relative density. This value can be consider as equal to the value of the lowest limit of the boundary region defined by Gupta, and nearly correspond to our results, according to the grain size distributions measured (Figs. 5 and 6).

It can be seen that changing the value of x, in the $Pb_3(VO_4)_{2(1-x)}(PO_4)_{2x}$ formula, has the effect of modifying both the rate and the densification mechanism. For an equal relative density before plot downturn,

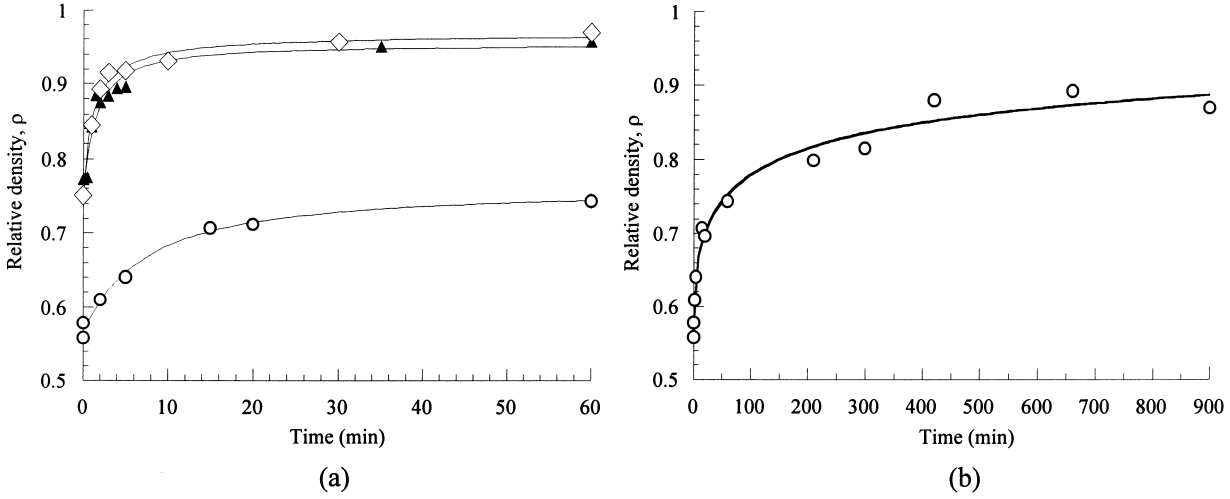

Fig. 2. Densification curves at 650°C for (a) (▲) $Pb_3(VO_4)_2$, (◇) $Pb_3(VO_4)_{1.6}(PO_4)_{0.4}$ and (○) $Pb_3(PO_4)_2$ samples up to 60 min, compared with densification behaviour for (b) (○) $Pb_3(PO_4)_2$ samples up to 900 min.

densification rate of $Pb_3(PO_4)_2$ is 100 times lower than in rich vanadium compounds. Beyond 90% of the theoretical density, densification rates for $Pb_3(VO_4)_2$ and $Pb_3(VO_4)_{1.6}(VO_4)_{0.4}$ tend to fall rapidly. In fact, once porosity begins pinching off in powder compacts, pressure of trapped air might strongly increase with ρ up to a level able to reduce densification rate in limiting the sintering driving force. Due to important role played by non-densifying mechanisms, such as surface diffusion or vapour-phase transport, $Pb_3(VO_4)_{2(1-x)}(PO_4)_{2x}$ grains are able to grow faster during intermediate-stage sintering. As reported by Bullard and Searcy,[12] similar phenomena were observed in LiF compacts. Important grain coarsening occurred because of surface diffusion, and gas entrapment in closed pores stopped densification above $\rho = 0.95$. Coble first pointed out the consequence of air trapped in pores in limiting densification.[13] When non-densifying mechanisms are less important, fully dense materials can be obtained, such as metals[14] and oxides.[15]

As shown in Fig. 6, pore isolation seems to have an impact on densification rate plots of $Pb_3(VO_4)_2$ and $Pb_3(VO_4)_{1.6}(VO_4)_{0.4}$ samples. On the other hand, $Pb_3(PO_4)_2$ pellets behave differently. First, at the end of sintering experiments, i.e. after 900 min of sintering at 650°C, powder compacts reached a relative density close to 90% of the theoretical one, below the achievement of pore closure according to Budworth. Indeed, in a theoretical model of pore closure based upon an assembly of truncated octahedra, Budworth predicted a pore breaking up at 8.4% of porosity,[16] as experimentally notified in typical ceramics like Al_2O_3[13,17,18] or BeO.[15]

It is possible to correlate the changes in slopes, by considering two densification mechanisms instead of one controlling-densification process. Indeed, Kuczinsky[19] was the first to consider simultaneous volume and grain boundary diffusion mechanisms of mass transport during sintering. Later, Johnson proposed a general model for intermediate-stage of sintering, both due to grain boundary and volume diffusion.[20–23] Also Rosolowski and Greskovich[24] developed a sintering model of both densification and grain growth in considering new calculation of vacancy flow from pores. They exposed a two terms expression for flow of vacancies of the rate-limiting species from a pore, and experimentally showed that in sintering of Al_2O_3, BeO and copper, one diffusion mechanism can be neglected to an other. At last, DeHoff [25] and Rhines and DeHoff [26] described a new sintering model based on geometrical considerations, i.e. microstructure evolution. Dominance by volume or grain boundary diffusion is determined by the grain boundary total length:total pore surface ratio. Then, if we can assume that during microstructure evolution, the predominant sintering mechanism can change, leading to different slopes in densification rate-relative density plots, the mechanism by which the pore network is broken has yet to be elucidated. Moreover, it is not clearly shown either one mechanism occurs after another or both mechanisms operate simultaneously with one dominating upon another.

Fig. 7 gives the relationship between grain size and relative density for the three different $Pb_3(VO_4)_{2(1-x)}(PO_4)_{2x}$ compounds. The grain-size-density trajectory is a function of the relative ratio of the densification rate to the grain growth rate.

It can be seen and confirm from theses trajectories that in spite of rapid densification for $Pb_3(VO_4)_2$ and $Pb_3(VO_4)_{1.6}(PO_4)_{0.4}$ (see Fig. 2), grain growth is more important in $Pb_3(VO_4)_2$ samples as shown above (Fig. 4). This difference in grain growth behaviour tends to explain why the densification rate $d\rho/dt$ for $Pb_3(VO_4)_{1.6}(PO_4)_{0.4}$ samples is higher than for $Pb_3(VO_4)_2$ samples.

All curves are linear until the density boundary region is reached ($88 \leqslant \rho \leqslant 90\%$). According to Figs. 6 and 7, during intermediate-stage sintering, it can be concluded

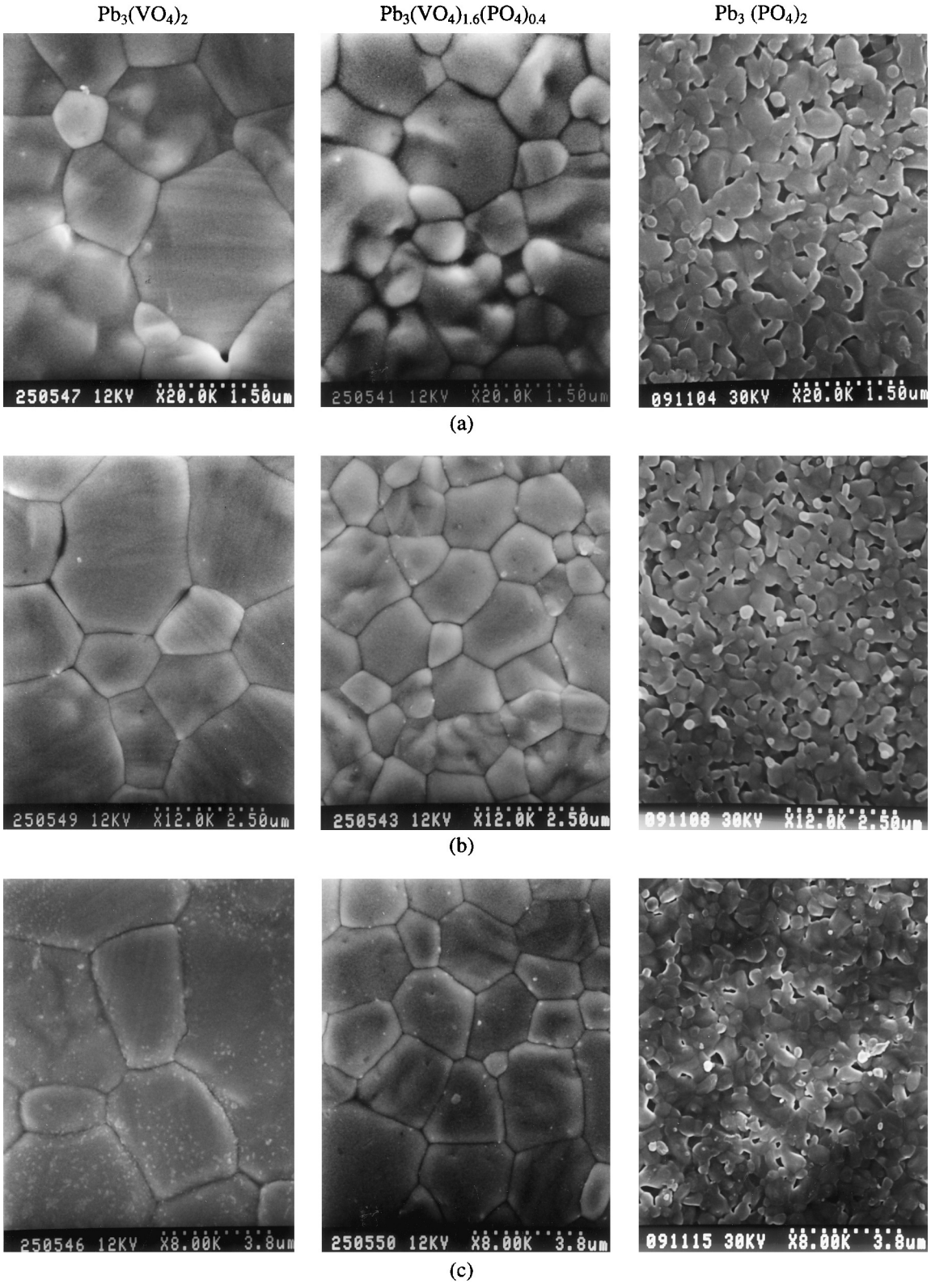

Fig. 3. Micrographs at 650°C for different sintering time: (a) 10 min, (b) 60 min and (c) 900 min.

that since vanadium concentration is high, i.e. when x is low, $d\rho/dt$ is strongly increased, in limiting grain growth mechanism. The flattering in $G-\rho$ trajectories, that is observed in phosphor-containing materials opposite $Pb_3(VO_4)_2$, reflects the fact that vanadium substitution enhances the densification rate:grain growth rate ratio. Interestingly, the $G-\rho$ curves for the non-pure vanadium materials, i.e. when $x \neq 0$, are quite similar until the pore

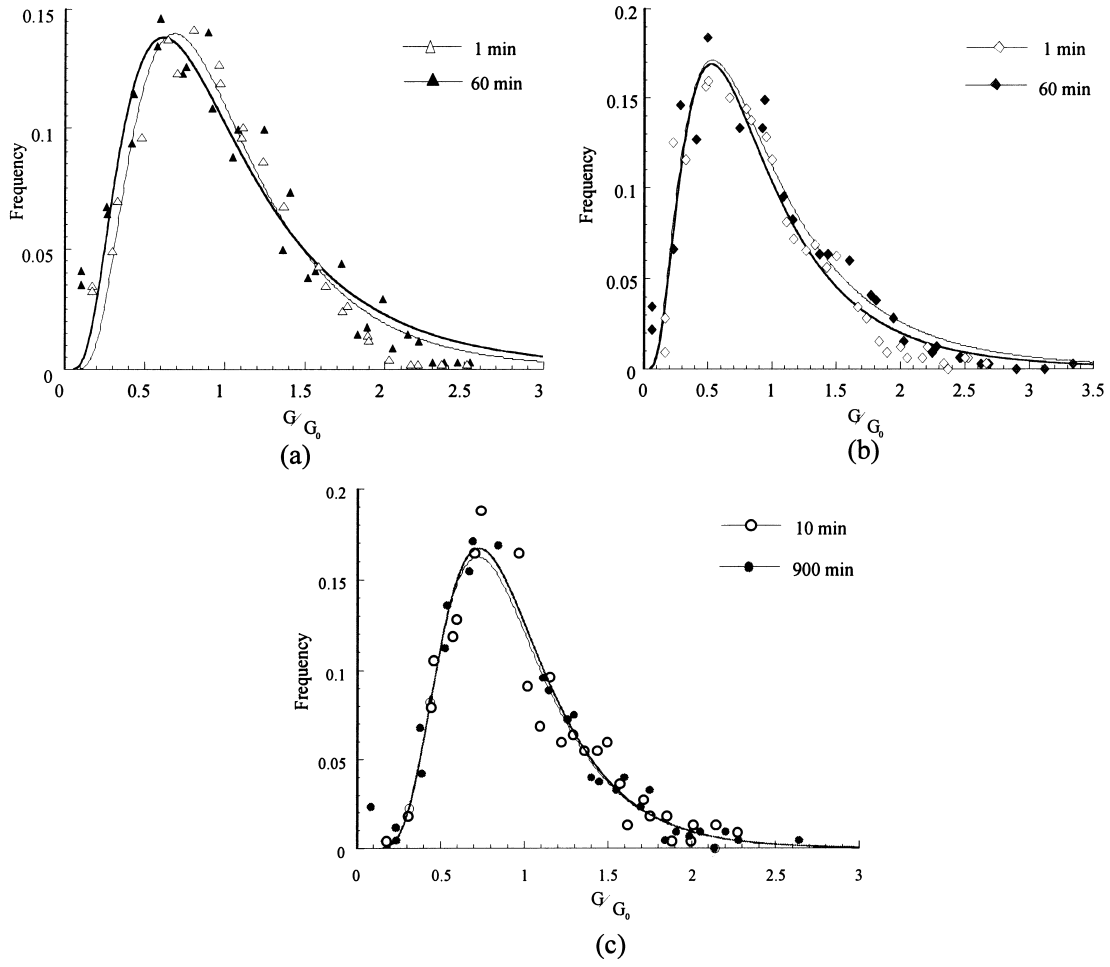

Fig. 4. Conservation of grain size distribution at 650°C for (a) (△) $Pb_3(VO_4)_2$, (b) (◇) $Pb_3(VO_4)_{1.6}(PO_4)_{0.4}$ and (c) (○) $Pb_3(PO_4)_2$ with log-normal law fittings.

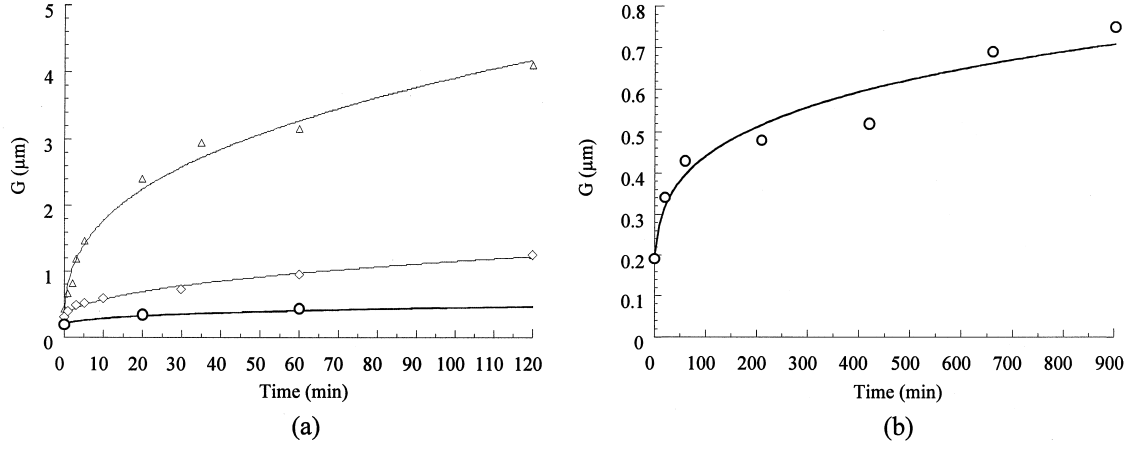

Fig. 5. Grain size as a function of sintering time at 650°C for (a) (△) $Pb_3(VO_4)_2$, (◇) $Pb_3(VO_4)_{1.6}(PO_4)_{0.4}$ and (○) $Pb_3(PO_4)_2$ samples up to 120 min, compared with grain growth behaviour for (b) (○) $Pb_3(PO_4)_2$ samples up to 900 min.

closure; this might be because the densification rate:grain growth rate ratio is quite similar for these two materials.

It is fair to conclude from $G-\rho$ curves (Fig. 7) that linear relations exist between density and grain size, following Gupta,[10] up to the density boundary region as defined in Fig. 6. Without any assumption on specific geometry, densification rate can be expressed as followed:[14]

$$\frac{d\rho}{dt} = \frac{AD}{(1-\rho)^{\alpha} G^{n}} \quad (1)$$

where $\frac{d\rho}{dt}$ is the densification rate, A a constant related to the controlling diffusion mechanism at a given temperature and D the diffusion coefficient. The grain size exponent n is predicted to be equal to 3 and $\alpha = 0$ for lattice-diffusion-controlled densification whilst for boundary-diffusion-controlled densification $n = 4$ and $\alpha = 1/2$.

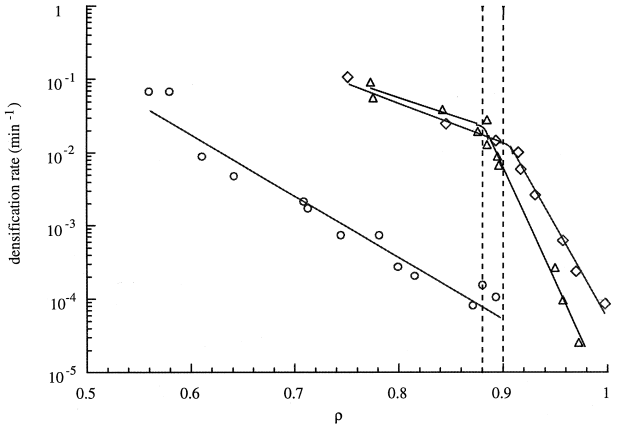

Fig. 6. Isothermal densification rate as a function of relative sintered density of (△) $Pb_3(VO_4)_2$, (◇) $Pb_3(VO_4)_{1.6}(PO_4)_{0.4}$ and (○) $Pb_3(PO_4)_2$ samples.

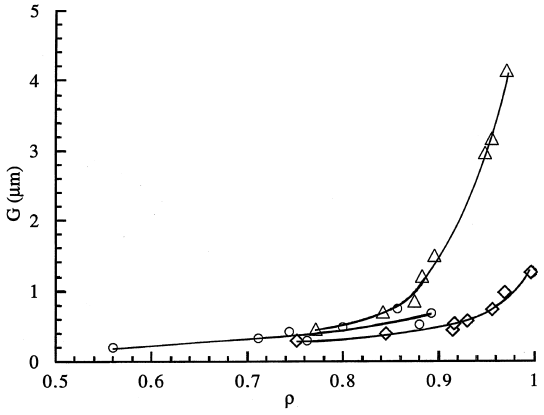

Fig. 7. Grain-size-density trajectory for (△) $Pb_3(VO_4)_2$, (◇) $Pb_3(VO_4)_{1.6}(PO_4)_{0.4}$ and (○) $Pb_3(PO_4)_2$ materials.

In order to understand the particle size dependence of the densification mechanisms, it is useful to plot the densification rate versus grain size for the 3 studied materials (Fig. 8).

The points corresponding to relative densities higher than 90% of the theoretical density — i.e. after pore closure — were excluded from consideration, because fitting with these data points belonging to final-stage sintering process was not reliable. Indeed, densification kinetics during final-stage sintering was found to be dependent of N_g, the number of pores per grain.[27] Moreover, grain growth above $\rho = 0.9$ becomes the predominant process, as shown in Figs. 2(a) and 7.

The densification rate-grain size exponents n are determined from the slopes in Fig. 8 using a least-squares analysis. On one hand, the densification exponent for $Pb_3(PO_4)_2$ is in a range of 4.0–4.5; it is fair to conclude it corresponds to a densification mechanism controlled by grain-boundary diffusion. Because coarsening of lead orthophosphate is very limited, densification rate:grain growth rate ratio is high. As a consequence, the fitting operation which gives grain-boundary diffusion as the densification mechanism is reliable. On the other hand, values for vanadium compounds are in a range of 5.5–6.5 for $Pb_3(VO_4)_{1.6}(PO_4)_{0.4}$ and 2.1 to 2.4 for $Pb_3(VO_4)_2$ samples. These exponents do not correspond to any densification mechanism. It seems to show that in these experimental conditions, densification is controlled by a mixed mechanism of lattice and grain-boundary diffusion. In fact, due to rapid densification behaviour as observed for $Pb_3(VO_4)_{1.6}(PO_4)_{0.4}$ and $Pb_3(VO_4)_2$, it is quite difficult to correlate experimental data to the densification rate Eq. (1). Hydroxyapatite behaviour is similar to those observed for $Pb_3(VO_4)_{1.6}(PO_4)_{0.4}$ and $Pb_3(VO_4)_2$ compounds.[28]

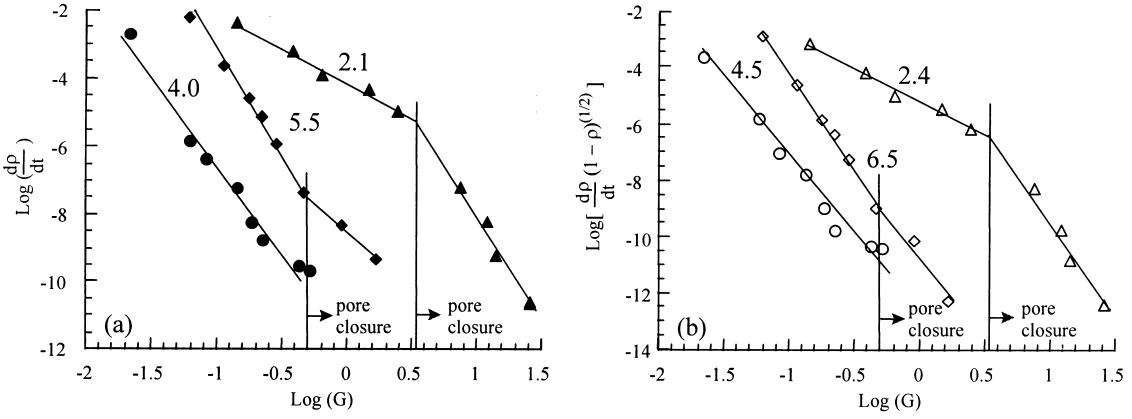

Fig. 8. Logarithm of densification rate with (a) $\log(\frac{d\rho}{dt})$ for lattice diffusion and (b) $\log\left[\frac{d\rho}{dt}(1-\rho)^{1/2}\right]$ for grain boundary diffusion versus logarithm of grain size. Samples represented are (▲,△) $Pb_3(VO_4)_2$, (◆,◇) $Pb_3(VO_4)_{1.6}(PO_4)_{0.4}$ and (●,○) $Pb_3(PO_4)_2$.

Other isothermal sintered materials such as hydroxyapatite $Ca_{10}(PO_4)_6(OH)_2$, are able to attain 95% of the theoretical density in less than 20 min, in a temperature range from 1000 to 1100°C. This fast densification observed in $Ca_{10}(PO_4)_6(OH)_2$ is also characterised by a high densification rate-grain size exponents n. Inversely, when densification mechanism is activated at high temperature such as undoped and MgO-doped Al_2O_3 samples, Berry and Harmer[20] have found good agreement for the sintering equation to data.

Moreover, when densification and grain growth occur during heating of the sample, the relative density and the grain size at 650°C facing green density and powder grain size are changed. Thus, because of mechanisms acting before desire temperature of 650°C is reached, it can be concluded that determination of the exponent observed for $Pb_3(VO_4)_{1.6}(PO_4)_{0.4}$ and $Pb_3(VO_4)_2$ can not be done with precision.

We have mentioned that changing the value of x in the $Pb_3(VO_4)_{2(1-x)}(PO_4)_{2x}$ formula is able to strongly modify densification mechanism. It was first put in light the impact on end-point density. Indeed, for small amount of phosphor, i.e. when x is equal to 0.2, it has been observed a improvement in final density, whereas the end-point density decreases a lot when x is equal to 1. Moreover, vanadium substitution tends to change the predominant rate for densification process, from fast- to low-densification behaviour (Fig. 6).

It is possible to resume some of these remarks in using Eq. (2). The condition that two powders of the same particle size but different degree of vanadium substitution should densify to the same extent at a given time and temperature is that:

$$\frac{d\rho/dt_{V-\text{low}}}{d\rho/dt_{V-\text{rich}}} \propto \frac{D_{V-\text{low}}}{D_{V-\text{rich}}} \tag{2}$$

where $d\rho/dt_{V-\text{rich}}$ and $d\rho/dt_{V-\text{low}}$ are the densification rates, and $D_{V-\text{rich}}$ and $D_{V-\text{low}}$ the diffusion coefficients of the limiting species. It follows that for a given size, when the densification rate ratio will increase, $D_{V-\text{low}}/D_{V-\text{rich}}$, the diffusion coefficient ratio, will increase as well. It has been observed in Fig. 8 that an increase of phosphor concentration in $Pb_3(VO_4)_{2(1-x)}(PO_4)_{2x}$ compounds, leads to of the decrease of densification rate resulting from a reduction in diffusion coefficient mentioned above. Thus, for $G = 0.6$ μm (see Fig. 8) when increasing the vanadium substitution with phosphor from $x = 0$ to $x = 1$, the diffusion coefficient ratio of the limiting species will decrease by a factor of 10^6. It's important to mention here that relative density for $Pb_3(VO_4)_2$ and $Pb_3(PO_4)_2$ when $G = 0.6$ μm are very different: $Pb_3(VO_4)_2$ begins to sinter and $Pb_3(VO_4)_2$ seems to reach its limiting relative density at this temperature.

4.2. Grain growth kinetics

Grain growth kinetics for both $Pb_3(VO_4)_2$ and $Pb_3(VO_4)_{1.6}(PO_4)_{0.4}$ are expressed by the same grain growth rate law:

$$\frac{dG}{dt} = \frac{K}{G^{m-1}} = \frac{K}{G^2} \tag{3}$$

where G is the grain size after sintering time t, and K a constant depending on the diffusion coefficient. The measured exponent value, close to $m = 3$ that is commonly observed in many ceramics, can correspond to at least five different mechanisms. So, the attachment of physical significance to this value is very dubious. Nevertheless, because of some grain boundary-pore separation without abnormal grain growth, and G greater than the pore radius, kinetics are boundary controlled mechanisms. But, neither coalescence of second phase by lattice diffusion, diffusion through continuous second phase, nor solute drag in a doped system can characterise gain growth mechanism for both $Pb_3(VO_4)_2$ and $Pb_3(VO_4)_{1.6}(PO_4)_{0.4}$. Indeed, as shown in Fig. 9, no second phase can be found in lead orthophosphovanadates compounds. For pure systems such as these, a deviation from $m = 2$ is often reported, and can be explained in terms of lost factors due to approximations

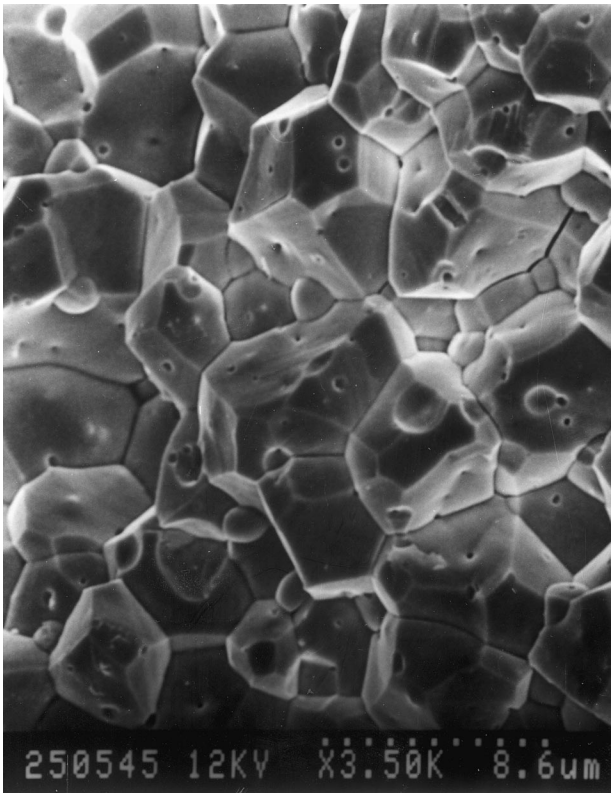

Fig. 9. Typical microstructure in lead orthophosphovanadates after 900 min at 650°C. No abnormal grain growth can be found as well as no second phase.

used in calculating this kind of grain growth equation giving m to be integer. So, grain growth kinetics in $Pb_3(VO_4)_2$ and $Pb_3(VO_4)_{1.6}(PO_4)_{0.4}$ compounds are controlled by grain boundaries in pure materials.

The grain-growth constant K were determined to be 5.1×10^{-1} and 1.6×10^{-2} μm^3/min, for $Pb_3(VO_4)_2$ and $Pb_3(VO_4)_{1.6}(PO_4)_{0.4}$ samples, respectively. Clearly, lowering vanadium concentration in substituted lead orthophosphovanadates reduces grain growth during the intermediate-stage sintering (Fig. 10).

In contrast, the present data for $Pb_3(PO_4)_2$ samples are in good agreement with a grain growth based on surface-diffusion-controlled pore drag (Fig. 11). In this model, the grain growth rate can be expressed by

$$\frac{dG}{dt} = \frac{CD_S}{G^3(1-\rho)^{4/3}} \quad (4)$$

where C is a constant, ρ the relative density and D_s the surface diffusion coefficient.

We observed that lowering the grain growth of $Pb_3(VO_4)_2$ in substituting vanadium by 20% of phosphor leads to a slight increase in the final density (see Fig. 2). Moreover, when studying grain growth during intermediate-stage sintering, it is to obvious to say that pores have a strong influence of the developing geometry during the sintering process,[29] especially in impeding grain boundary movement.[30] Then, the evolution in porosity collapsing during isothermal sintering leads to modify the grain growth kinetics in changing the surface tension. It seems we can assume that relative density has strong influence on grain growth. As well, it has been precisely shown that narrower the pore-size distribution, stronger the effects on limiting grain growth.[31,32] Moreover, pore-boundary separation can be stopped when distribution in pores is homogeneous and tight.[33] As a final remark, it's expected that grain growth laws are not valid when density changes, with a simultaneous pore drag.[34–36] As densification and grain growth are linked together, grain-size exponents depend on microstructure evolution during densification. All previous works referenced below clearly put in the light how difficult is to determinate the grain growth mechanism during densification. However, in order to identify such a mechanism without any ambiguity, further work, such as grain growth in fully dense or pore-size controlled materials, should be conducted.

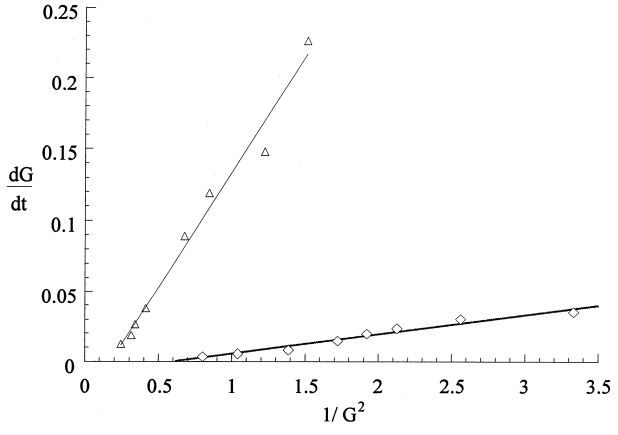

Fig. 10. Grain-growth kinetics during sintering for (△) $Pb_3(VO_4)_2$ and (◇) $Pb_3(VO_4)_{1.6}(PO_4)_{0.4}$.

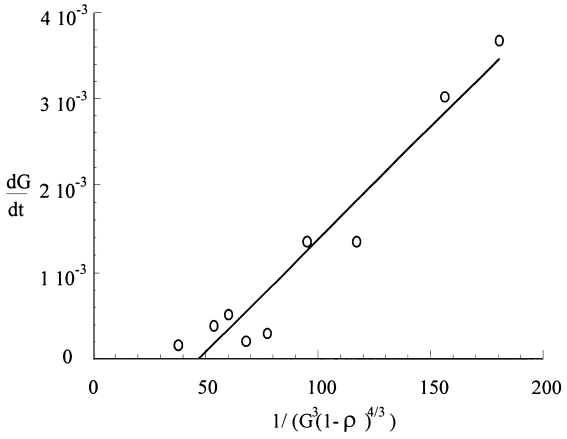

Fig. 11. Grain growth rate, plotted according to the model for surface-diffusion-controlled pore drag for $Pb_3(PO_4)_2$.

It is possible to take into account the grain growth rate as another parameter, to highlight the vanadium substitution dependence on grain boundary mobility. Fig. 12 shows the densification rate:grain growth rate ratio as a function of grain size.

Presence of phosphor enhances densification prior to grain growth (ratio >1) in the intermediate-stage sintering, while for phosphor free compound, grain growth is at least 10 times faster than densification. It can be concluded that vanadium substitution by phosphor improve densification during intermediate-stage sintering, and limits grain growth. As a consequence, boundary mobility slows down, preventing pore-boundary separation.

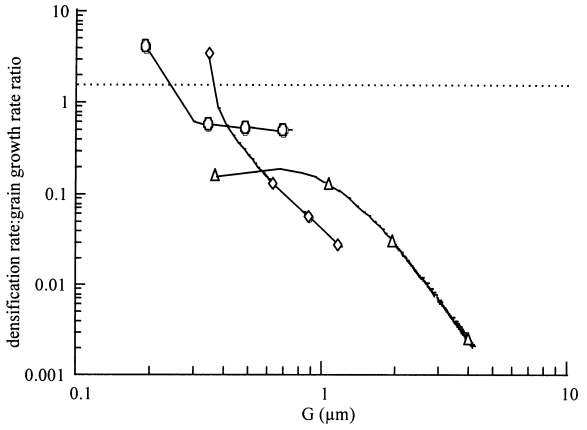

Fig. 12. Densification rate:grain growth rate ratio versus grain size for (△) $Pb_3(VO_4)_2$, (◇) $Pb_3(VO_4)_{1.6}(PO_4)_{0.4}$ and (○) $Pb_3(PO_4)_2$ materials.

5. Conclusions

Three lead orthophosphovanadates compositions were sintered at 650°C. In rich-phosphor compound, i.e. $Pb_3(PO_4)_2$, the densification kinetic during the intermediate-stage sintering was consistent with grain-boundary diffusion being the controlling mechanism, whereas in rich vanadium compounds ($Pb_3(VO_4)_{1.6}(PO_4)_{0.4}$, and $Pb_3(VO_4)_2$) densification seemed to occur by a mixed mechanism of lattice and grain-boundary diffusion. For the two compounds which contains vanadium, it has been shown that grain growth kinetics were controlled by grain boundary but without being able to precise the grain growth mechanism. Whilst, it was shown that grains of $Pb_3(PO_4)_2$ grew by a surface diffusion controlled mechanism. Above the sintering characteristics, it clearly appeared that changing the value of x in $Pb_3(VO_4)_{2(1-x)}(PO_4)_{2x}$ considerably modified the sintering mechanism, both the densification path and the diffusion coefficient of the limiting species. Lowering the vanadium concentration both reduced densification rate and grain growth rate. In fact, it has been shown that the decrease in grain growth rate is more important than the densification rate reduction with substituting vanadium element. Further work with new compositions is in progress, in order to study grain growth for dense ceramics.

References

1. Carpena, J. and Lacout, J. L., Procédé de conditionnement de déchets radioactifs utilisant des apatites silicatées comme matrice de confinement, French Patent 08676, 1993.
2. Audubert, F., Mise au point d'une matrice apatitique pour le confinement de l'iode 129. PhD thesis, INP Toulouse, 1995.
3. Audubert, F., Carpena, J., Lacout, J. L. and Tetard, F., Elaboration of an iodine-bearing apatite: iodine diffusion into a $Pb_3(VO_4)_2$ matrix. *Solid State Ionics*, 1997, **95**(1–2), 113–119.
4. Carpena, J., Audubert, F. and Lacout, J. L., Procédé de conditionnement de l'iode 129 utilisant une apatite comme matrice de confinement, French Patent 14706, 1994.
5. Robin, T., Bernache-Assollant, D. and Audubert, F., Influence of grinding method on $Pb_3(VO_4)_{1.6}(PO_4)_{0.4}$ sinterability. *Powder Tech.*, in press.
6. Kiat, J. M., Etude par diffraction des rayons X des états métastables générés au cours des transitions de phases du niobiate de barym et de sodium et des phosphovanadates de plomb: influence des défauts et des coexistences de phases. Ph.D thesis, Université Pierre et Marie CURIE, Paris VI, 1988.
7. Fullman, R. L., Measurement of particle sizes in opaque bodies. *Trans. AIME*, 1953, **197**, 447–452.
8. Garnier, P., Calvarin, G., Berar, J. F. and Weigel, D., Etude des phases ferroélectriques de $Pb_3V_2O_8$: détermination de la maille cristalline de la phase ã ferroélectrique basse température. *Mat. Res. Bull.*, 1984, **19**, 407–414.
9. Kiat, J. M., Garnier, P., Calvarin, G. and Pinot, M., Structural study of lead orthophosphovanadates: role of the electron lone pairs in the phases transitions. *J. Solid State Chem.*, 1993, **103**, 490–503.
10. Gupta, T. K., Possible correlation between density and grain size during sintering. *J. Am. Ceram. Soc.*, 1972, **55**(5), 276–277.
11. Shiau, F.-S., Fang, T.-T. and Leu, T.-H., Effect of particule-size distribution on the microstructural evolution in the intermediate stage of sintering. *J. Am. Ceram. Soc.*, 1997, **80**(2), 286–290.
12. Bullard, J. W. and Searcy, A. W., Microstructural development during sintering of lithium fluoride. *J. Am. Ceram. Soc.*, 1997, **80**(9), 2395–2400.
13. Coble, R. L., Sintering crystalline solids: II, experimental test of diffusion models in powder compacts. *J. Appl. Phys.*, 1961, **32**(5), 793–799.
14. Coble, R. L. and Gupta, T. K., Intermediate stage sintering. In *Sintering and related phenomena*, ed. G. C. Kuczinski, New York, 1967, pp. 423–441.
15. Clare, T. E., Sintering kinetics of beryllia. *J. Am. Ceram. Soc.*, 1966, **49**(3), 159–165.
16. Budworth, D.W., Theory of pore closure during sintering. *Trans. Br. Ceram. Soc.*, 1970, **69**(1), 29–31.
17. Ikegami, T. and Moriyoshi, Y., Intermediate-stage sintering of a homogeneously packed compact. *J. Am. Ceram. Soc.*, 1984, **67**(3), 174–178.
18. Cameron, C. P. and Raj, R., Grain-growth transition during sintering of colloidally prepared alumina powder compacts. *J. Am. Ceram. Soc.*, 1988, **71**(12), 1031–1035.
19. Kuczinski, G. C., Self diffusion in sintering of metallic particles. *Trans AIME*, 1949, **185**, 169–178.
20. Berry, K. A. and Harmer, M. P., Effect of MgO solute on microstructure development in Al_2O_3. *J. Am. Ceram. Soc.*, 1986, **69**(2), 43–49.
21. Johnson, D. L., New method of obtaining volume, grain-boundary, and surface diffusion coefficients from sintering data. *J. Appl. Phys.*, 1969, **40**(1), 192–200.
22. Johnson, D. L., A general model for the intermediate stage of sintering. *J. Am. Ceram. Soc.*, 1970, **53**(10), 574–577.
23. Kumar, P. and Johnson, D. L., Sintering of CoO: II, intermediate stage. *J. Am. Ceram. Soc.*, 1974, **57**(2), 65–68.
24. Rosolowski, J. H. and Greskovich, C., Theory of the dependence of densification on grain growth during intermediate-stage sintering. *J. Am. Ceram. Soc.*, 1975, **58**(5–6), 177–182.
25. DeHoff, R. T., A cell model for microstructural evolution during sintering. In *Sintering and Heterogeneous Catalysis*. 1984, pp. 23–34.
26. Rhines, F. N. and DeHoff, R. T., Channel network decay in sintering. *Mat. Sci. Res.*, 1984, **16**, 49–61.
27. Zhao, J. and Harmer, M. P., Effect of pore distribution on microstructure development: III, Model experiments. *J. Am. Ceram. Soc.*, 1992, **75**(4), 830–843.
28. Ababou, B., Etude expérimentale et théorique du préfrittage et du frittage de l'hydroxyapatite $Ca_{10}(PO_4)_6(OH)_2$. Thesis, Université de Limoges, 1994.
29. Kingery, W. D. and Francois, The sintering of crystalline oxides, I. Interactions between grain boundaries and pores. In *Sintering and related phenomena*, ed. H. G. Kuczinski, New York, 1967, pp. 449–466.
30. Burke, J. E, Grain growth. In *Cermaic microstructures*, ed. R.M. Fulrath and J.A. Pask. New York, 1968, 681–700.
31. Harmer, M. P. and Zhao, J., Effect of pores on microstructure development. In *Ceramic microstructures '86: Role of interfaces*, New York, 1986, pp. 455–464.
32. Zhao, J. and Harmer, M. P., Effect of pore distribution on microstructure development: I, matrix pores. *J. Am. Ceram. Soc.*, 1988, **71**(2), 113–126.
33. Yan, M. F., Cannon, R. M. J., Bowen, H. K. and Chowdhry, U., Effect of grain size distribution on sintered density. *Mat. Sci. Eng.*, 1983, **60**, 275–281.
34. Brook, R. J., Pore-grain boundary interactions and grain growth. *J. Am. Ceram. Soc.*, 1969, **52**(1), 46–57.
35. Brook, R. J., Controlled grain growth. In *Treatise on materials science*, New York, 1976, pp. 331–334.
36. Carpay, F. M. A., Discontinous grain growth and pore drag. *J. Am. Ceram . Soc.*, 1977, **60**(1-2), 82–83.